Received: 26 May 2020 | Accepted: 3 July 2020

DOI: 10.1002/maco.202011839

ARTICLE

Materials and Corrosion

Exfoliation and intergranular corrosion resistance of the 2198 Al–Cu–Li alloy with different thermomechanical treatments

João V. de Sousa Araujo[1] | Mariana X. Milagre[1] | Raphael O. Ferreira[2] | Caruline de Souza Carvalho Machado[1] | Aline de Fátima Santos Bugarin[1] | Izabel F. Machado[2] | Isolda Costa[1]

[1]Materials Science and Technology Center, Nuclear and Energy Research Institute–IPEN/CNEN-SP, São Paulo, São Paulo, Brazil

[2]Surface Phenomena Laboratory, Polytechnic School of the University of São Paulo, São Paulo, São Paulo, Brazil

Correspondence
João V. de Sousa Araujo, Nuclear and Energy Research Institute–IPEN/CNEN-SP, Av. Prof. Lineu Prestes, 2242, São Paulo, SP, Brazil.
Email: joao-neutron@hotmail.com

Funding information
Fundação de Amparo à Pesquisa do Estado de São Paulo, Grant/Award Number: 2019/18388-1

Abstract

In this study, the resistance to exfoliation and intergranular corrosion (IGC) of the 2198 Al–Cu–Li alloy submitted to different thermomechanical treatments (T3, T8, and T851) was investigated. The tests were carried out following the standard practices, ASTM G34-18 and ASTM G110-15, respectively. All the tested alloys showed susceptibility to exfoliation and some alloys showed susceptibility to IGC, but the artificially aged alloys presented a higher tendency to exfoliation. The extensive hydrogen evolution reaction (HER) was observed on the surfaces of artificially aged alloys when immersed in the EXCO solution. The HER resulted in an increase in solution pH with the time of immersion. Also, the weight losses related to the artificially aged alloys were higher than that of the naturally aged ones. The T8 treatment was the only condition that resulted in susceptibility to both, intergranular and transgranular corrosion, whereas the T851 treatment did not show IGC susceptibility, only transgranular corrosion. Finally, the 2198-T3 condition showed the highest corrosion resistance among the thermomechanical treatments tested. The results of the 2198 alloy subjected to various treatments were compared with that of the 2024-T3 alloy. This last alloy showed higher resistance to exfoliation and IGC as compared with the 2198 alloy.

KEYWORDS

Al–Cu–Li alloys, exfoliation corrosion, intergranular corrosion, thermomechanical treatments, transgranular corrosion

1 | INTRODUCTION

Exfoliation and intergranular corrosion (IGC) are common types of localized corrosion in Al alloys. Exfoliation is described as a kind of IGC, usually associated with rolled materials and extruded materials, and sometimes forged materials, with elongated grains.[1] IGC is associated with an attack at grain boundaries or their vicinities when the second phase is precipitated there. The second phase might act as anodic or cathodic sites in relation to Al matrix, depending on their chemical composition.[2] The attack might propagate along the grains or at their adjacent regions.[3] Both types have been reported as common corrosion morphologies in metals.[4,5] In the last

few decades, the susceptibility of Al alloys to exfoliation and IGC has been studied.[6–15] Some works showed that these attacks are harmful to aircraft structures.[16–19] Consequently, many research studies have been developed to understand the influence of Al alloys' microstructural features in the propagation of these kinds of corrosion morphologies.[20–26] The effects of the fabrication process[27–31] and heat treatment[32–41] on the microstructural features, and thus on the corrosion behavior are commonly investigated.

Keddam et al.[42] studied the corrosion behavior of the 2024-T351, 2219-T87, and 6013-T6 Al alloys by electrochemical impedance spectroscopy measurements in the EXCO solution. The corrosion rates in these alloys initially increased (during the first 6 hr of test), but it was followed by a progressive decrease in the corrosion rate, until the end of test (48 hr). This phenomenon was attributed to variation in the cathodic reaction kinetics during the progress of test and also to the different microstructural features of each alloy.

Yue et al.[43] studied the corrosion resistance of the 2195 Al–Li alloy submitted to rolling deformation in different directions. It was verified that the main causes of IGC and exfoliation corrosion were the precipitation of second phases, as T1 (Al_2CuLi) and θ′ (Al_2Cu), which led to galvanic coupling between the precipitate-free zones and the matrix. Moreover, according to the authors, exfoliation corrosion occurred preferentially on the surface parallel to the rolling direction. In contrast, Zhou et al.[10] reported that IGC corrosion susceptibility in the 2024 (Al–Cu) and 2099 (Al–Cu–Li) alloys is related to the grains with relatively high levels of defects, in which second phases are absent.

Yan et al.[44] investigated the effect of artificial aging at 155°C and 200°C on the IGC susceptibility of the 2050 Al–Cu–Li alloy. The high IGC corrosion susceptibility was correlated with Li segregation at the grain boundaries, which increases with the aging temperature. Huang et al.[45] compared the effect of heat treatment and the predeformation on the 1460 alloy containing 0.12 wt% Li. The authors monitored the IGC development at the open circuit potential (OCP). A diagram correlating aging time with OCP curves was proposed. According to authors, the alloy was susceptible to four types of attacks, depending on the potentials, such as pitting with IGC (−0.50 to −0.64 V vs. saturated calomel electrode [SCE]), which was characterized by pits associated with deeper IGC; general IGC (−0.64 to 0.68 V vs. SCE) associated with pits and shallow IGC; local IGC (−0.68 to −0.71 V vs. SCE), in which the attack is centralized in a specific area; and pitting (−0.72 to −0.77 V vs. SCE) characterized by a type of attack close to the surface.

Machado et al.[27] and Milagre et al.[20] studied the IGC and exfoliation development in two different types of Al–Cu–Li alloys welded by friction stir welding (FSW). It was verified that susceptibility to these forms of corrosion changed according to the microstructural features of each FSW zone, such as grain size and dissolution of strengthening phases. Recently, Peng et al.[46] examined the effect of aging treatment on the susceptibility to IGC and exfoliation corrosion of the Al–Cu–Li–Zr–Sc alloy. Three different stages of aging were investigated: (a) single-stage aging, where the samples were given heat treatment at 160°C; (b) strain aging, where the samples were submitted to a predeformation (cold work) of 3.5% and heat treatment at 160°C; and (c) double-stage aging, in which the samples were submitted to 3.5% of predeformation (cold work) and heat treatment at 160°C for 2 hr, followed by heat treatment at 160°C for 24 hr. It was verified that the alloy submitted to single-stage aging at 160°C showed the best corrosion resistance due to its lower amount of T1 precipitation at the grain boundaries.

The literature[4] has reported that susceptibility of the Al alloys to IGC and exfoliation can be influenced by different factors, such as manufacturing process and microstructural features. The 2198 alloy has been proposed as a potential replacement of alloy 2024 due to its higher fatigue resistance.[47] It is applied in aircraft structures with the T3, T8, and T851 tempers on beams or seat rails, skins, and cradle frame, respectively.[48,49] The search for mechanical properties leads to different treatments used according to the mechanical property necessary to the specific material application. However, the choice of temper according to application usually does not take into account the damage that these materials might cause due to limited corrosion resistance if they are used in improper tempers.[50] The corrosion susceptibility of age-hardened Al–Cu–Li alloys (such as T8 and T851) when compared with the naturally hardened alloys (T3), is known[50] due to the heterogeneous microstructure of the age-hardened alloys when compared with the fairly uniform microstructure related to the T3 alloy. Usually, T3-tempered aluminum alloys exhibit improved corrosion resistance in comparison to age-hardened alloys; these last ones with numerous precipitates form a large number of galvanic cells. However, a comparison of the effect of artificial aging on the resistance to IGC and EXCO of Al–Cu–Li alloys, specifically the 2198 Al–Cu–Li alloy, comparing the aged-hardened with naturally aged alloys, has not yet been studied. Considering the importance of the resistance to exfoliation and IGC in alloys used in aircrafts, this study aims to fill this gap. In this study, the susceptibility of the 2198 Al–Cu–Li alloy to exfoliation and IGC corrosion submitted to different thermomechanical treatments was investigated following the

ASTM G34-2018[51] and the ASTM G110-2015[52] standard practices. The mechanisms of corrosion propagation observed for each temper condition were described. Finally, a comparison of the susceptibilities of the different tempers of the 2198 Al–Cu–Li alloy to IGC and exfoliation with the most commonly used Al alloy in aircraft structures, the commercial 2024-T3 Al-Cu alloy, was carried out once the Al–Cu–Li alloys were proposed to replace the Al–Cu ones. The main contribution of this manuscript is to clarify the effect of the temper on the susceptibility to IGC and exfoliation, with a relation between weight loss and pH being clearly established in the EXCO solution. Besides, information about the corrosion attack depth in the IGC solution is discussed. This information has great importance for the aeronautical industry, as failures of these materials caused by corrosion might lead to fatal aircraft accidents in the operating condition.

2 | EXPERIMENTAL

2.1 | Materials

Alloys 2024-T3 and 2198 in the commercially available tempers, T3, T8, and T851, were investigated. The chemical composition of each alloy is presented in Table 1.

The T3 temper corresponds to a sequence of solution heat treatment, cold working, and natural aging steps. The T8 temper comprises a solution heat treatment step, a cold working step, and an artificial aging step. Finally, the T851 temper encompasses solution heat treatment, stress relief by stretching, and artificial aging. The Al–Cu alloy 2024 does not contain lithium and is the conventional material used in T3 temper in aircraft applications.[49] The intention is to compare the resistance against exfoliation and IGC of a material that is largely used with a material that intends to replace it. The thicknesses of the different types of Al materials used are shown in Table 2.

TABLE 1 The chemical composition (wt%) of the alloys obtained by inductively coupled plasma optical emission spectrometry

	Alloys			
		2198		
Elements	2024-T3	T3	T8	T851
Cu	4.50	3.24	3.34	3.31
Li	–	1.02	0.95	0.96
Mg	1.41	0.30	0.31	0.31
Mn	0.61	0.01	0.02	0.01
Fe	0.12	0.04	0.05	0.04
Zn	0.03	0.02	0.04	0.01
Al	Balance			

TABLE 2 Thickness of the alloy plates used in this study

Alloys	Thickness (mm)
2024-T3	1.5
2198-T3	3.2
2198-T8	4.0
2198-T851	1.6

2.2 | Evaluation of susceptibility to exfoliation corrosion (according to ASTM G34)

2.2.1 | Electrochemical characterization

Electrochemical characterization was carried out by OCP measurements in the EXCO test solution at room temperature ($22 \pm 2°C$) during 48 hr of immersion using an $Ag/AgCl_{KClsat}$ electrode as a reference electrode.

2.2.2 | pH measurements

The pH of the electrolyte was measured during the period of immersion in the EXCO solution using a Mettler Toledo® pH meter.

2.2.3 | Inductively coupled plasma optical emission spectrometry (ICP-OES) measurements

The electrolyte composition was analyzed by a Spectro model Arcos® with the axial torch and Meinhard® nebulizer. Aliquots of 10 ml of the EXCO solution were separated from the volume of the test solution and transferred to plastic flasks after different periods of immersion, and then they were subsequently analyzed for Al, Cu, Li, Mg, and Fe by ICP-OES.

2.2.4 | Weight loss measurements

Weight loss measurements were carried out to monitor the corrosion rate of the 2198 alloy with the various tempers and the 2024-T3 alloy as a function of time of immersion. Samples of these alloys were weighed before the test and after the samples were removed from the

solution, cleaned in an ultrasonic bath, and dried. Extra samples were used to evaluate the mass loss after different periods of immersion.

2.2.5 | Exfoliation corrosion test

Exfoliation corrosion tests were performed according to ASTM G34-2018.[51] The samples were immersed in a solution composed of 4-mol/L NaCl + 0.5-mol/L KNO_3 + 0.1-mol/L HNO_3 and distilled H_2O up to 1 L for 48 hr. The ratio of electrolyte volume/sample surface was 30 ml/cm^2. During the testing, 100 ml of solution was used in all samples. This solution is known as the EXCO test solution. This standard is mostly used in aircraft industries in a routine quality control procedure, which will serve as a reference to comparison with other works in the literature.

2.3 | IGC test (according to ASTM G110)

IGC tests were performed according to ASTM G110-2015.[52] Samples of the tested alloys were cleaned in a mixture of 945-ml distilled H_2O, 50-ml HNO_3 (70%), and 4-ml HF (48%) for 1 min at 93°C. Subsequently, the samples were exposed for 1 min in the HNO_3 solution (70%) at room temperature. Then, they were immersed in a solution with 1-mol/L NaCl and 10 ml of H_2O_2 (30%) diluted with distilled H_2O up to 1 L. The period of exposure for this solution, at room temperature, corresponded to 6 hr.

2.4 | Microstructural characterization

After the immersion tests, the cross-section of the corroded samples was observed by scanning electron microscopy (SEM) using a TM Model 3000 and JEOL JSM-6010LA microscope, equipped with an energy-dispersive X-ray spectroscopy (EDX) detector.

3 | RESULTS

3.1 | Results from exfoliation corrosion testing

3.1.1 | OCP variation with time in the EXCO solution

Figure 1 shows the surface of the tested Al alloys after 16 hr of exposure to the EXCO solution. Larger amounts of hydrogen bubbles were seen on the surface of the 2198 alloy with T8 and T851 tempers, compared with T3. H_2 bubbles' evolution is observed at the cathodic sites and the amount of bubbles is proportional to the susceptibility of the alloy to corrosion, indicating higher susceptibility to exfoliation of the artificially aged alloys.[20,53,54] These results are also in agreement with the variation of OCP with the time of immersion (Figure 2). For the 2024-T3 alloy, the electrode potential initially shifted toward nobler values, likely due to ennoblement of the alloy resulting from the selective dissolution of the most active elements, such as Mg, Mn, and Al, but it soon shifted back into the direction of more negative values, which could be due to removal of the ennobled precipitates from the surface,[55] mainly those located at the grain boundaries or inside the grains. Also, it was accompanied by precipitation of insoluble corrosion products at the attacked surface. The potential achieved fair stabilization after around 6 hr in the EXCO solution. This phenomenon was also observed in a previous work.[42] For the 2198-T3, a similar behavior was observed in the first hours of immersion; however, after an initial potential drop (nearly 1 hr of the test), it increased slowly and reached stability after 24 hr of immersion. The slow corrosion kinetics related to the T3 temper, due the lower amount of hardening precipitades, was already

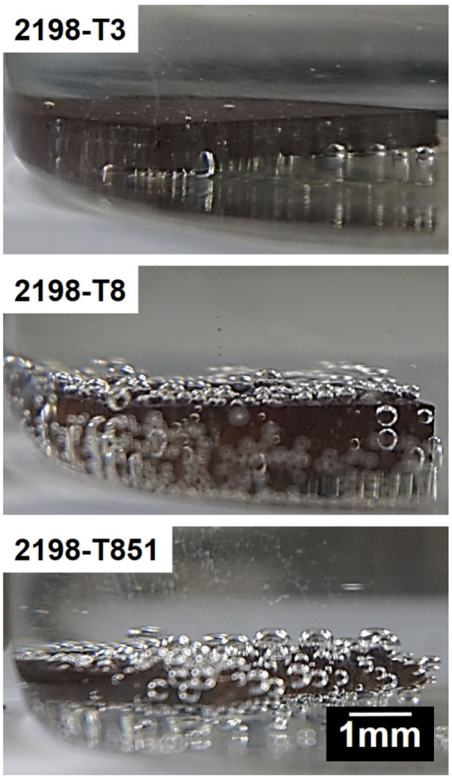

FIGURE 1 Macrograph images of the 2198 alloys in the T3, T8, and T851 conditions after 16 hr of immersion in the EXCO solution (4-mol/L NaCl + 0.5-mol/L KNO_3 + 0.1-mol/L HNO_3 in 1 L of distilled H_2O)

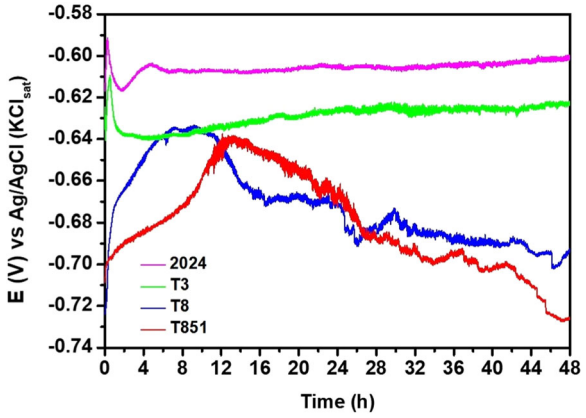

FIGURE 2 The open circuit potential curves of the alloys obtained during 48 hr of immersion in the EXCO solution (4-mol/L NaCl + 0.5-mol/L KNO_3 + 0.1-mol L HNO_3 in 1 L of distilled H_2O) [Color figure can be viewed at wileyonlinelibrary.com]

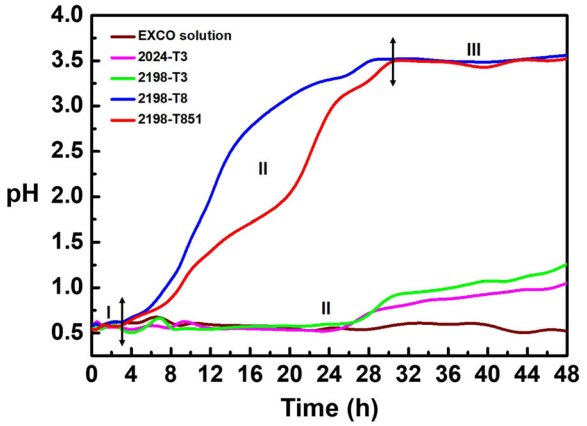

FIGURE 3 Monitoring of the EXCO solution pH during 48 hr of immersion test [Color figure can be viewed at wileyonlinelibrary.com]

reported in previous works[50] and, consequently to their slower kinetics and electrochemical activities as compared with the T8 and T851 tempers. For these two last tempers, the initial potentials were more negative than for the alloys with T3 temper due to the lower electrochemical activity related to this last temper. For T8 and T851, the potential largely increased with time and the rate of potential increase was faster for the T8 alloy as compared with T851; both reached a maximum potential, followed by a potential decrease after approximately 10 and 12 hr of immersion, respectively, in the test solution. Relative to the artificially aged alloys, the T851 temper presented a greater potential variation than the T8, which is likely due to the higher amounts of precipitates in T851. More stable potentials were found for the 2024-T3 and 2198-T3 in the EXCO solution due to their higher electrochemical stability as compared to the 2198 with the T8 and T851 tempers.

3.1.2 | pH monitoring in the EXCO solution

The pH curves were recorded during 48 hr in the EXCO test (Figure 3). According to the pH range, the curves were classified into three stages that were dependent on the type of alloy. At the initial periods of immersion in the EXCO solution (Stage I), pH was in the range 0.6–0.7 for all alloys, and during this period, it was proposed that the predominant mechanism was the selective dissolution of the more active elements in the alloy. This resulted in an increased concentration of cations (Li and/or Mg and Al) in the solution, promoting water hydrolysis, followed by hydrogen evolution, and consequently pH increase. The large volumes of hydrogen bubbles formed on the artificially aged Al alloy samples led to a significant pH increase from the pH range of 0.7–3.5 for the artificially aged tempers, 2198-T8 and 2198-T851, between nearly 4 and 26 hr of exposure to the EXCO solution (Stage II). For the naturally aged tempers, 2024-T3 and 2198-T3, the pH increase was delayed, starting after approximately 26 hr and not before testing was finalized. The differences between the behaviors related to the tempers are due to the electrochemical activity of these alloys that result in hydrogen gas production. Finally, Stage III for the artificially aged alloys (2198-T8 and 2198-T851) corresponded to the pH range between 3.5 and 3.6 and potential stability, which must be due to surface coverage by hydrogen bubbles. For the alloys with T3 temper, however, pH slowly increased during Stage III, and it was in the range 0.8–1.2; also, the potential gradually increased, but at a low rate, which might be related to only partial coverage of the exposed surface with hydrogen bubbles. These results show that besides a lower electrochemical activity in the T3 temper, the kinetics of this electrochemical activity was also slower as compared with the T8 and T851 tempers.

3.1.3 | The elemental analysis of the EXCO solution

The results of EXCO solution analysis after various periods of immersion of samples, obtained by ICP-OES, are shown in Figure 4. Larger concentrations in the test solution corresponded to aluminum ions (hundreds of times larger compared with the other elements) in the solution, and it increased with time since the first hour of immersion and continuously increased throughout the test. The next elements in order of concentration in the solution were Li, in the case of the 2198 alloy, and Mg, in the case of the 2024

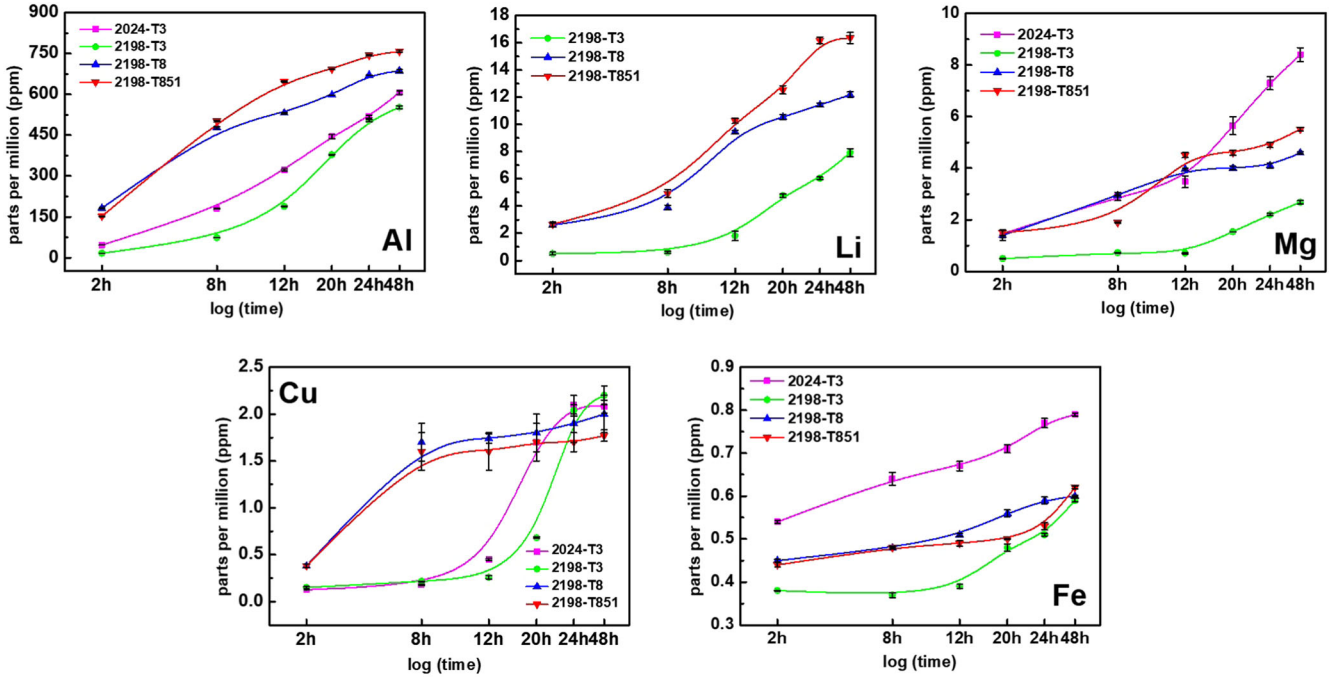

FIGURE 4 Monitoring of the EXCO solution composition during 48 hr of immersion test by inductively coupled plasma optical emission spectrometry [Color figure can be viewed at wileyonlinelibrary.com]

alloy. However, it must be noted that Mg was also dissolved from the 2198 alloy with the various tempers (T3, T8, and T851) in significant amounts. The kinetics of elements' dissolution in the EXCO solution was similar to 2198-T3 and 2024-T3, for most elements, with the exception of Mg and Li, for obvious reasons, as Li was not present in the 2024 and Mg was found in significantly lower amounts in the 2198 alloy, compared with 2024 alloy. The results suggest similarities in the kinetics of the dissolution of the 2024-T3 and 2198-T3 alloys, indicating the effect of the temper on the corrosion kinetics. Iron concentration was also analyzed in the solutions, but it was always below 1 ppm for all tested alloys.

The results also show that the large pH variation is accompanied by the high rate of increase in Mg and Li ions in the solution until 8–12 hr for the 2198-T8 and 2198-T851 alloys, supporting the hypothesis that selective dissolution of these elements is the main cause of potential increase and also the faster increase of pH in this period. The pH continues to increase after this time of test for both alloys, but at slower rates. The lower increments in Li content were observed fot the 2198-T3. In another hand, lower increments of Mg were observed for 2024-T3. However, a continuous increase along with the test for these samples explains the continuous increase in potential and pH related to these alloys. As for the Cu content in solution, it is interesting to note the differences between the kinetics of dissolution between the artificial and natural tempers, and the similarities between similar tempers, even if the composition differs, as is the case of 2024 and 2198.

3.1.4 | Weight loss measurements

A direct correlation between weight loss and pH variation was established in the EXCO solution, as shown in Figure 5. Both the curves, that of pH and of weight loss, follow the same profile. Tempers corresponding to artificial aging (T8 and T851) were related to greater pH increase and larger weight losses.

3.1.5 | Exfoliation corrosion behavior

After EXCO test, the cross-section morphologies of each alloy tested were analyzed by SEM.

Susceptibility to exfoliation was not indicated in the 2024-T3 alloy (Figure 6). In addition, corrosion initiation apparently is related to intermetallic particles and its propagation to intergranular attack, as indicated by arrows in Figure 6a. At higher magnifications (Figure 6b), these features, intergranular attack propagation and corrosion attack at the vicinity of the intermetallic particles, are also pointed by red arrows and are seen below the outer surface, indicating that propagation is caused by an IGC attack. A similar behavior has been reported in other works.[29,42,56]

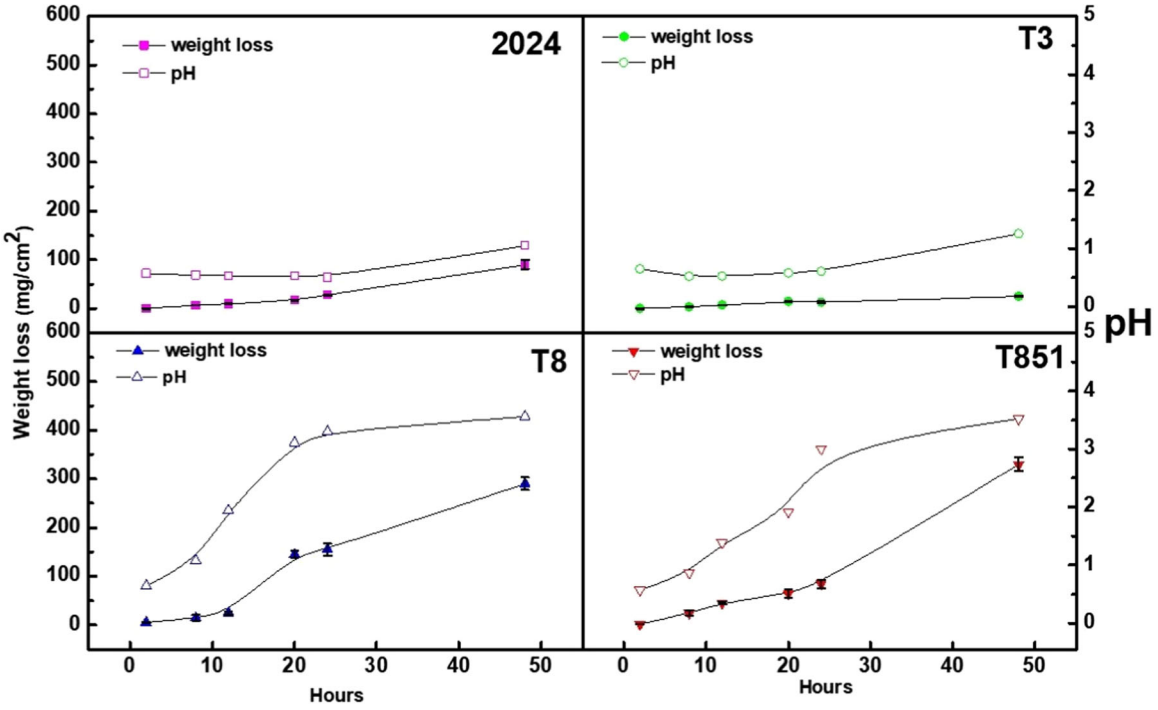

FIGURE 5 The relation between pH increment and weight loss during 48 hr of immersion in the EXCO solution (4-mol/L NaCl + 0.5-mol/L KNO_3 + 0.1-mol/L HNO_3 in 1 L of distilled H_2O) [Color figure can be viewed at wileyonlinelibrary.com]

Exfoliation susceptibility was indicated for 2198-T3 (Figure 7a). Despite the exfoliation susceptibility of this alloy, a comparison with 2024-T3 shows that in this last alloy, the corrosion attack penetrated deep into the thickness of the plate (Figure 6a); for the 2198-T3 alloy (Figure 7b), the attack occurred at the outer layers of the surface and along the rolling direction (yellow arrow). The artificially aged alloys tested for exfoliation tendency, 2198-T8 and 2198-T851, presented susceptibility to this type of attack (Figures 8 and 9, respectively).

In both overaged tempers of this alloy, attack propagation penetrated deep into the thickness, as indicated by arrows in Figures 8a and 9a. A common feature observed after exposure of both artificially aged alloys to the EXCO solution was the transgranular attack, as illustrated by Figures 8b and 9b. In Figure 10, some of the corrosion features are presented. It is observed that some grains are preserved (grain A) and others are attacked (grain B). Moreover, for the T8 condition, the attack occurred along the deformation direction (blue arrow, Figure 10a), whereas for the T851 temper, the preferential attack occurred at slip bands, as indicated by the yellow arrow (Figure 10b) within the most active grains. This type of attack has been related to slip bands by other

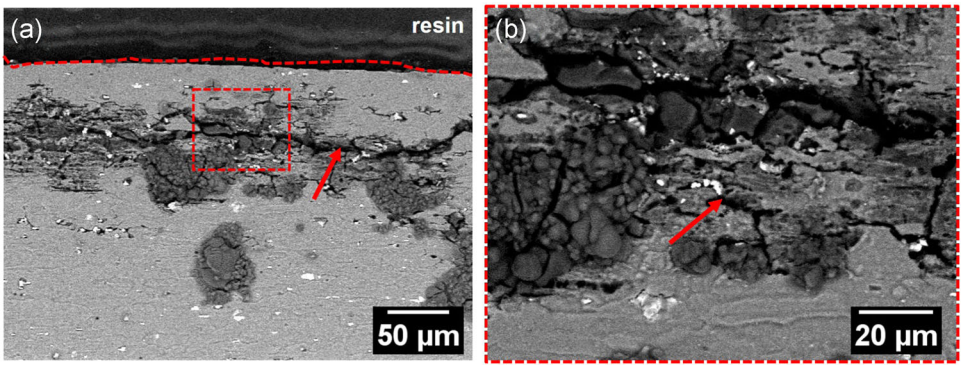

FIGURE 6 (a) A cross-section image of the 2024-T3 alloy after 48 hr of immersion in the EXCO solution (4-mol/L NaCl + 0.5-mol/L KNO_3 + 0.1-mol/L HNO_3 in 1 L of distilled H_2O). (b) Higher magnification of the squared region in (a). The arrows indicate the attack along grain boundaries [Color figure can be viewed at wileyonlinelibrary.com]

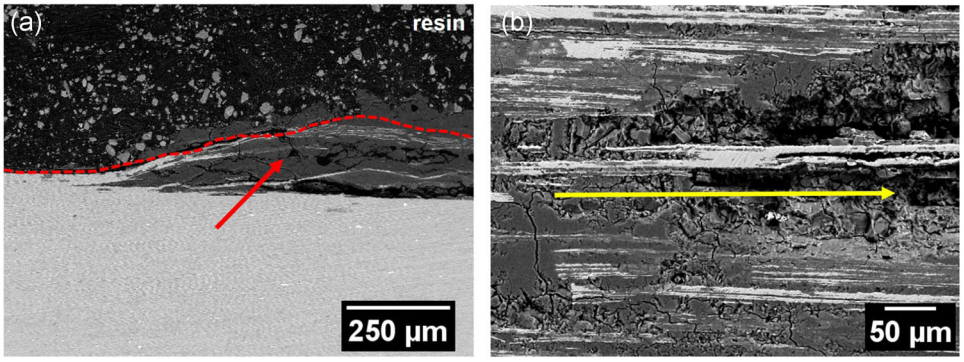

FIGURE 7 (a, b) Cross-section images of different regions of the 2198-T3 alloy after 48 hr of immersion in the EXCO solution (4-mol/L NaCl + 0.5-mol/L KNO_3 + 0.1-mol/L HNO_3 in 1 L of distilled H_2O).The red and yellow arrows indicate the attack in the exfoliation region and in the rolling direction, respectively [Color figure can be viewed at wileyonlinelibrary.com]

authors.[50,57–60] Grain boundaries were preserved for T851, as shown by red arrows in Figure 9a,b and also in Figure 10a,b. Analyses by EDX maps in the areas of heavy corrosion attack in 2198-T851 (Figure 11) showed copper enrichment at the borders of the attacked areas, indicating that elements more active than Al are dissolved from the alloy.

3.2 | Results of IGC testing

3.2.1 | IGC behavior

Figure 12 shows SEM cross-section images of samples of the 2024-T3 (Figure 12a) and 2198 alloy with the T3 (Figure 12b), and T851 (Figure 12c,d) tempers after the standard test for IGC. All the samples showed a selective corrosion attack at grain boundaries in this solution. The 2024-T3 alloy clearly showed susceptibility to IGC (Figure 12a). According to the literature,[61,62] this type of attack in this alloy is related to the S phase (Al_2CuMg) precipitated at the grain boundaries. For the 2198-T3 alloy, IGC susceptibility was indicated (Figure 7). It is likely that precipitation of T1 phase or other phases occurs preferentially at the grain boundaries of this alloy. However, for the artificially aged 2198 alloys, a transgranular attack predominated in both alloys, T8 and T851 (Figure 12c,d), instead of IGC. In the 2198-T851 alloy (Figure 12d), the transgranular attack was related to slip bands (yellow arrow), as also observed after the exfoliation test.

In the 2198-T8 sample (Figure 13), two types of corrosion were identified, IGC near the surface (red arrow, Figure 13a) and transgranular attack, deep inside the alloy (yellow arrow). At larger magnification (Figure 13b), this effect is more evident.

The depth of penetration attack was estimated for the tested alloys (Figure 14). The average of corrosion attack penetration for the 2198-T851 alloy was around 74 ± 25 µm, which is about twice of that corresponding to 2024-T3 and 2198-T3 (Figure 14a). As in the 2198-T8 alloy, two types of attacks—intergranular and transgranular—were observed,

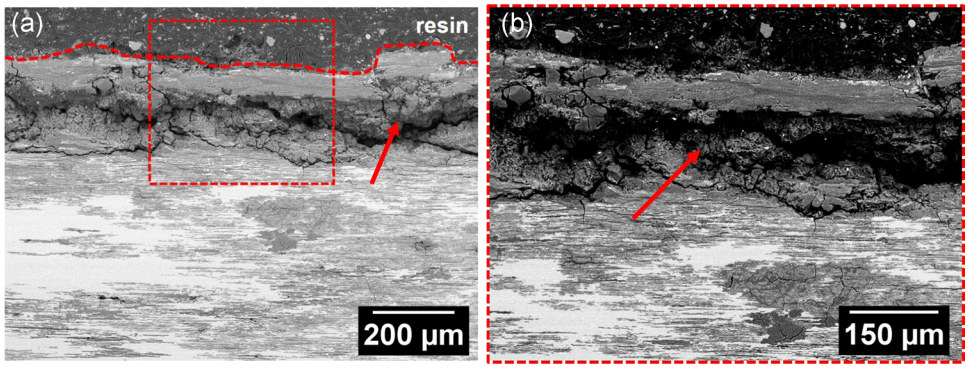

FIGURE 8 (a) A cross-section image of the 2198-T8 alloy after 48 hr of immersion in the EXCO solution (4-mol/L NaCl + 0.5-mol/L KNO_3 + 0.1-mol/L HNO_3 in 1 L of distilled H_2O). (b) Higher magnification of the squared region in (a). The arrows indicate an exfoliated region [Color figure can be viewed at wileyonlinelibrary.com]

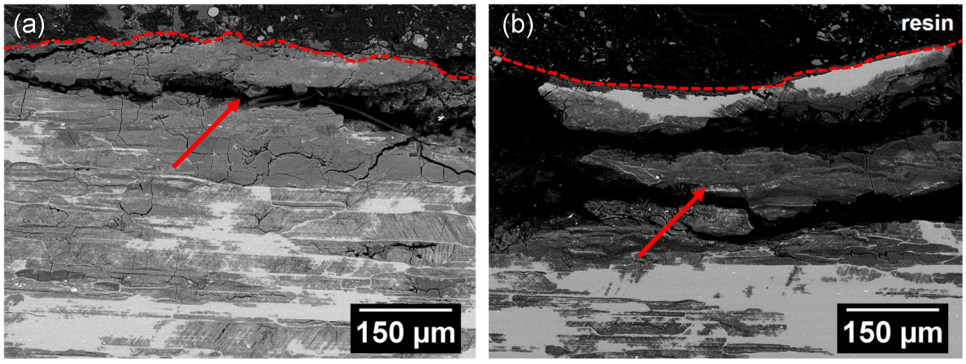

FIGURE 9 (a, b) Cross-section images of different regions of the 2198-T851 alloy after 48 hr of immersion in the EXCO solution (4-mol/L NaCl + 0.5-mol/L KNO_3 + 0.1-mol/L HNO_3 in 1 L of distilled H_2O). The arrows indicate the exfoliation region [Color figure can be viewed at wileyonlinelibrary.com]

the penetration corresponding to each type was estimated (Figure 14b). The mean depth of penetration equivalent to transgranular attack was around 45 ± 9 µm, whereas that corresponding to IGC was nearly 15 ± 6 µm. The maximum depth of attack penetration was also estimated for each tested alloy, and the results were 47 µm (2024-T3), 58 µm (2198-T3), 96 µm (2198-T8), and 140 µm (2198-T851). Taking into consideration the thickness of the plates, the mean penetration depths correspond to approximately 3% (2024-T3), 2% (2198-T3), 2% (2198-T8), and 11% (2198-T851) of plate's thickness. The analysis by EDX maps was also performed for 2198 artificially aged alloys (T8 and T851) after the IGC test, as shown in Figure 15. Cu enrichment was associated with the areas of intense corrosion attack that occurred preferentially inside the grains of these alloys. In the case of the 2198-T8 alloy, copper enrichment occurred at sites of transgranular attack (A) rather than at sites of IGC (B), showing that transgranular corrosion predominated in this alloy.

4 | DISCUSSION

It is interesting to note that in the EXCO solution, the electrochemical behavior of the naturally aged alloys, 2024-T3 and 2198-T3, presented similarities, despite the significant differences between these two alloys in all the main alloying elements. In contrast, their behavior was different from the other two tested tempers of the 2198 Al–Cu–Li alloy, T8 and T851, which showed a similar behavior. These results suggest that for the tested alloys, the temper conditions are more important for their corrosion behavior than their chemical composition. In the 2198 alloy, the main phases responsible for localized corrosion are the micrometric Al–Cu–Fe intermetallic phase and the nanometric precipitate T1(Al_2CuLi) phase.[57] In both alloys tested in the naturally aged tempers, 2024-T3 and 2198-T3, the corrosion behavior is mainly determined by the presence of micrometric phases in the two alloys. Taking into consideration that

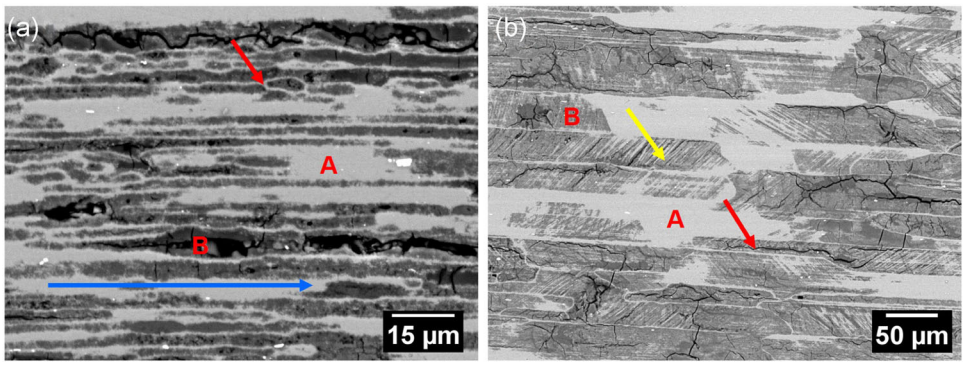

FIGURE 10 Cross-section images of 2198 alloy after 48 hr of immersion in the EXCO solution (4-mol/L NaCl + 0.5-mol/L KNO_3 + 0.1-mol/L HNO_3 in 1 L of distilled H_2O). (a) 2198-T8; (b) 2198-T851. The letters "A" and "B" represent different attacked and non-attacked regions, respectively. The yellow, red, and blue arrows represent corroded bands, grain boundary preservation, and deformation direction, respectively [Color figure can be viewed at wileyonlinelibrary.com]

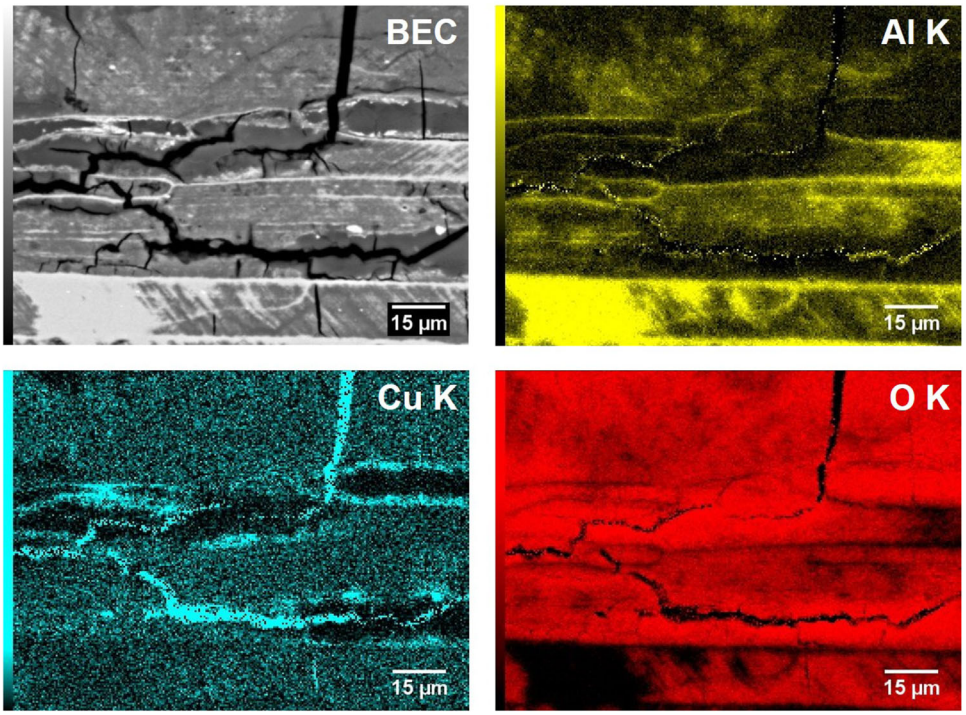

FIGURE 11 Energy-dispersive X-ray spectroscopy maps showing Cu redeposition at the grain boundaries of corroded grains in AA2198-T851 after 48 hr of immersion in the EXCO solution (4-mol/L NaCl + 0.5-mol/L KNO_3 + 0.1-mol/L HNO_3 in 1 L of distilled H_2O) [Color figure can be viewed at wileyonlinelibrary.com]

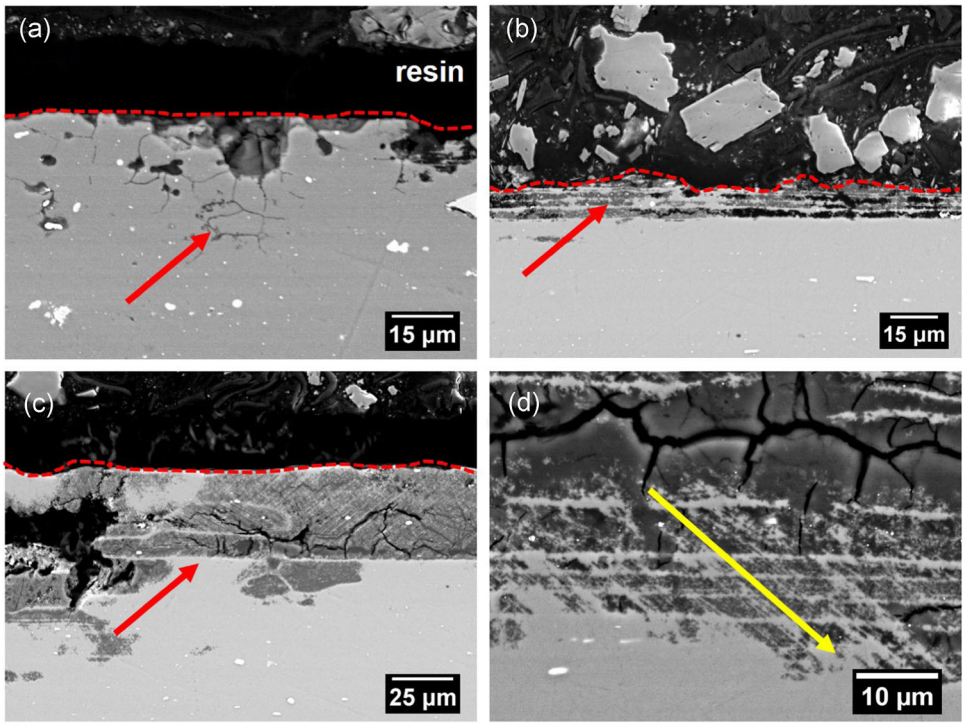

FIGURE 12 Cross-section images of the alloys after 6 hr of immersion in the intergranular corrosion solution composed of 1 mol/L of NaCl + 10 ml of H_2O_2 (30%) diluted in 1 L of distilled H_2O. (a) 2024-T3; (b) 2198-T3; (c,d) 2198-T851 in less and higher magnification, respectively [Color figure can be viewed at wileyonlinelibrary.com]

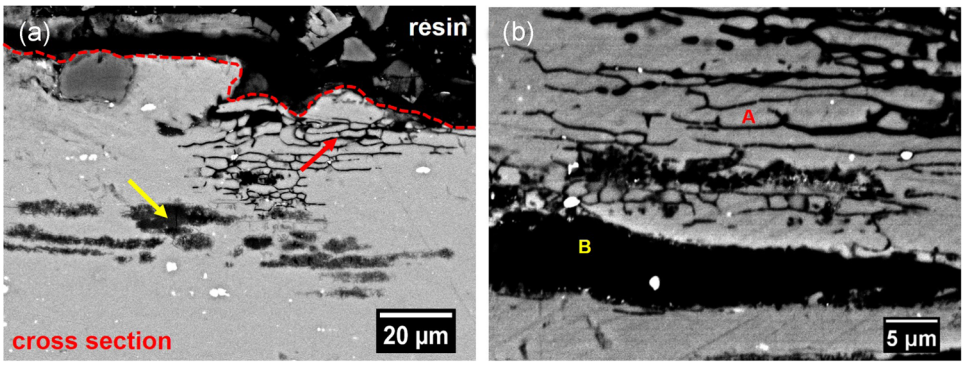

FIGURE 13 (a) Scanning electron microscopy images of 2198-T8 alloy after intergranular corrosion solution test; (b) high magnification. The arrows and "A" and "B" regions indicate intergranular and transgranular attacks [Color figure can be viewed at wileyonlinelibrary.com]

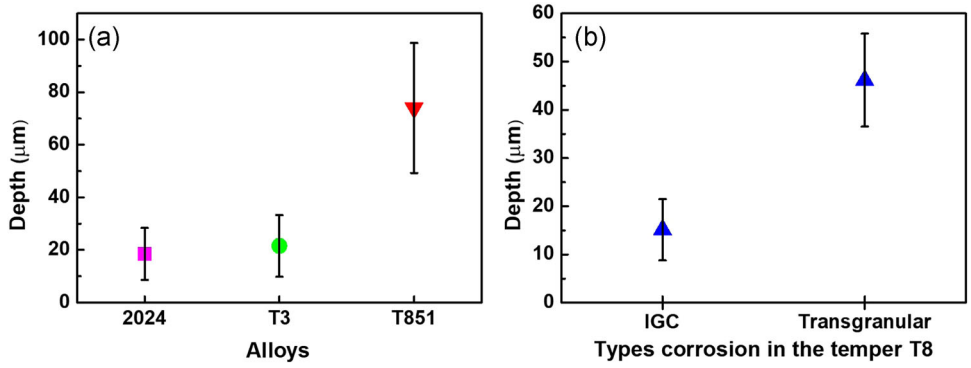

FIGURE 14 The depth of attack propagation for the tested alloys after 6 hr of immersion in the intergranular corrosion solution (1 mol/L of NaCl + 10 ml of H_2O_2 (30%) diluted in 1 L of distilled H_2O). (a) A comparison between the 2024-T3, 2198-T3, and 2198-T851 alloys, and (b) a comparison of the depth of the intergranular and transgranular attack in the 2198-T8 alloy [Color figure can be viewed at wileyonlinelibrary.com]

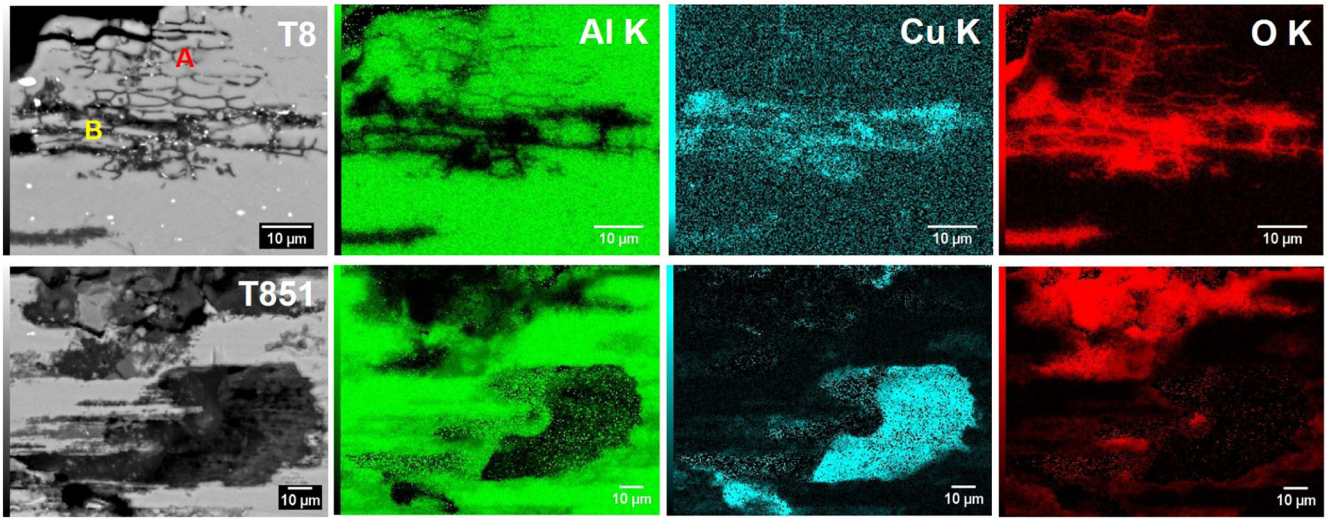

FIGURE 15 Energy-dispersive X-ray spectroscopy maps of the 2198-T8 and 2198-T851 alloys after 6 hr of immersion in the intergranular corrosion solution (1 mol/L of NaCl + 10 ml of H_2O_2 (30%) diluted in 1 L of distilled H_2O). The "A" and "B" regions indicate the sites of intergranular and transgranular attacks in the 2198-T8 alloy, respectively [Color figure can be viewed at wileyonlinelibrary.com]

natural and artificial aging influence precipitation of the T1 phase (Al_2CuLi) in Al–Cu–Li alloys, this phase was considered to be mainly responsible for localized corrosion in the artificially aged Al–Cu–Li alloys.[63] A recent work[50] showed, by differencial scanning calorimetry curves, that the tempers T8 and T851 have a higher density of T1 phase when compared with the T3 temper. This explains the similarities in the electrochemical behaviors of the T8 and T851 alloys, despite the differences in the corrosion kinetics of these two tempers (Figures 1–5). The main difference between the artificially aged (T8 and T851) and the naturally aged ones (T3) is indicated in the figures of potential and pH variation with time of the test. This occurs much faster in the artificially aged ones as compared with the naturally aged ones. These observations are seemingly related to the release of Al and Li into the solution, due to the corrosion attack of the T1 phase in large amounts in the T8 and T851 tempers (Figures 2 and 3). The Al and Li contents related to the start in pH increase are, respectively, above 450 ppm and 5 ppm. According to Figures 2 and 3, these amounts need to be exceeded to a significant pH increase. This observation applies to the 2198 alloys. For the 2024-T3 alloy, the increase in pH was related to the contents of Al and Mg, corresponding to values above 450 and 7 ppm, respectively. On the basis of these results, it might be proposed that whereas in the naturally aged alloys, the selective corrosion is predominantly related to the micrometric intermetallic phases and the corrosive attack related to these phases, in the case of the 2024, it is mainly associated with the S phase (Mg-rich), anodic to the matrix, and to the Al–Fe–Mn micrometric particles, cathodic to the matrix, which lead to trenching. The corrosion kinetics of the corrosion attack results in a slow release of the elements responsible for pH change, that is, Al, Li, and Mg. These observations are supported by the results presented in Figure 5 that show weight loss with time for the alloys and tempers tested.

It is worth noting that susceptibility to the types of corrosion attacks varied for the alloy 2198 from temper to temper. The naturally aged alloys, 2024-T3 and 2198-T3, presented susceptibility to IGC, which is related to the fact that the main nanometric phases, the S phase and T1 phase, respectively, in these alloys are located preferentially at their grain boundaries. However, for the age-hardened tempers of the Al–Cu–Li alloy, 2198-T8 and 2198-T851, transgranular corrosion predominated, even though susceptibility to IGC was also found for the T8 alloy. Both tempers, T8 and T851, presented a high tendency to exfoliation. This observation leads to the conclusion that the usual statement "all exfoliation corrosion is intergranular but not all IGC lead to exfoliation" is not correct for all aluminum materials. In fact, selective transgranular corrosion attack leads to high susceptibility to exfoliation. This is explained in the case of the alloys used in this study by the fact that the T1 phase is predominantly precipitated inside the grains. The 2024-T3 alloy, however, did not show susceptibility to exfoliation, despite the susceptibility to IGC related to the phase S located at the grain boundaries. The corrosion potentials of the T1 and S phases were described by Buchheit et al.[64] The authors reported that in 6 mol/L of NaCl, the potential of T1 phase is −0.2 V inferior to that of the S phase. This explains the higher kinetics of electrochemical reactions for the artificially aged alloys, with large amounts of T1 phase, compared with the naturally aged ones. This also elucidates the slower variation of pH along with the test for the naturally aged alloys, compared with the artificially aged ones (Figure 3). The amount of H_2 bubbles (Figure 1) and the content of elements dissolved in the EXCO solution (Figure 4) corroborate the results that showed higher corrosion susceptibility for the artificially aged alloys.

The results of the present work also showed how slight variation in the thermomechanical treatment, as between T8 and T851, might lead to a change in the corrosion mechanism, as it was observed during EXCO test. Whereas for the 2198-T851 alloy, the attack that resulted in exfoliation was transgranular, for the 2198-T8 alloy, the main type of attack varied with the depth of attack. Intergranular and transgranular attacks were seen at the outer layers of the alloy, whereas transgranular attack predominated higher depths of corrosion (Figure 13). Exfoliation in the 2198-T3 alloy (Figure 7) was related to the direction of grain deformation. Similar results were observed for the 2195 Al–Li alloy submitted to different levels of deformation.[43] The transgranular attacks in the 2189-T8 and 2198-T851 alloys occurred due to selective dissolution of particular grains that were more active due to their higher density of T1 phase, compared with others. Consequently, galvanic coupling occurred between grains with different amounts of T1 phase,[8,50,65] as observed in the EXCO and IGC tests (Figures 9, 10, 13a,b, and 14).

The pH monitoring during immersion tests showed the reason behind the relation of 2198-T851 alloy with high amounts of hydrogen bubbles (Figure 1). Hydrogen evolution during the corrosion process of Al–Cu–Li alloys has been reported in literature.[20,53,54,66] The H_2 bubbles represent the susceptibility to corrosion attack in the highly aggressive solution of EXCO test. The bubbles also exert pressure along the path of selective corrosion, leading to separation of grains and consequently formation of holes. Indeed, higher susceptibility to exfoliation was related to the alloys with larger amounts of H_2 bubbles at the surface.

The Cu enrichment was related to the regions of strong corrosion attack in the T8 and T851 alloys, which is explained by the selective dissolution of the most active elements, specifically Li and Al. This enrichment might accelerate corrosion propagation due to the formation of microcells between the copper-enriched sites and their vicinity. This is indicated by the areas of copper enrichment and their neighborhood, clearly observed for the 2198-T851 alloy (Figure 15). A similar tendency was observed for the alloys in the IGC standard test solution. Larger depths of the attack were associated with T851 and T8 tempers, and mainly with T851 that was related to the deepest corrosion penetration, corresponding to around 11% of the original thickness. This is the reason why intense investigation and testing of materials is a standard procedure of aircraft industry before they replace an alloy in their production by a new one.

5 | CONCLUSIONS

1. All tested 2198 alloys presented susceptibility to exfoliation, but the degree of susceptibility was dependent on the temper, with the T3 temper being related to the lowest susceptibility and the T851 temper to the highest. These results indicated the effect of T1 phase on the susceptibility to this type of selective attack.
2. The 2024-T3 alloy showed susceptibility to IGC but not to exfoliation; consequently, this alloy is more resistant to this type of corrosion than the 2198 alloy with various tempers.
3. The main type of corrosion attack associated with the age-hardened 2198 alloys was transgranular attack. For the 2198-T8 alloy, two types of corrosion were observed, intergranular near the surface and transgranular in areas deep into the plate.
4. The higher electrochemical activities in the EXCO solution for the artificially aged alloys, compared with the naturally aged ones, led to a large pH variation of the test solution.
5. The highest depth of corrosion penetration was related to the T851 temper, showing how variations in thermomechanical process affect the susceptibility of Al–Cu–Li alloys to localized corrosion.

ACKNOWLEDGMENTS

The authors are grateful to CNPq (2017-9/169569) and FAPESP (2013/13235-6 and 2019/18388-1) for financial support and the grant of J. V. S. A. They also acknowledge CAPES for the grant to M. X. M. (88882.333479/2019-01). Authors are also thankful to Dr. Marycel Elena Barboza Cotrim and Dr. João Cristiano Ulrich from CEQMA (IPEN/CNEN-SP) for the ICP-OES analyses.

ORCID

João V. de Sousa Araujo http://orcid.org/0000-0001-6375-0480
Mariana X. Milagre http://orcid.org/0000-0003-2048-2863
Caruline de Souza Carvalho Machado http://orcid.org/0000-0003-4172-119X

REFERENCES

[1] K. S. Prasad, N. E. Prasad, A. A. Gokhale, *Microstructure and Precipitate Characteristics of Aluminum-Lithium Alloys*, Elsevier Inc., London **2013**.
[2] S. C. Wang, M. J. Starink, *Int. Mater. Rev.* **2005**, *50*, 193.
[3] S. Zhang, W. Zeng, W. Yang, C. Shi, H. Wang, *Mater. Des.* **2014**, *63*, 368.
[4] C. Vargel, M. Jacques, M. P. Schmidt, *Corrosion of Aluminium*, Elsevier Inc., London **2004**.
[5] I. L. Muller, J. R. Galvele, *Corros. Sci.* **1977**, *17*, 179.
[6] J. Li, Z. Zhang, J. Zhang, C. Cao, J. Chinese Soc, *Corros. Prot.* **2003**, *23*, 319.
[7] M. Guérin, E. Andrieu, G. Odemer, J. Alexis, C. Blanc, M. Guérin, E. Andrieu, G. Odemer, J. Alexis, C. Blanc, *Corros. Sci.* **2014**, *85*, 455.
[8] M. Guérin, J. Alexis, E. Andrieu, L. Laffont, W. Lefebvre, G. Odemer, C. Blanc, *Corros. Sci.* **2016**, *102*, 291.
[9] V. Proton, J. Alexis, E. Andrieu, J. Ô. Delfosse, A. Deschamps, F. De Geuser, M. C. Lafont, C. Blanc, *Corros. Sci.* **2014**, *80*, 494.
[10] X. Zhou, C. Luo, Y. Ma, T. Hashimoto, G. E. Thompson, A. E. Hughes, P. Skeldon, *Surf. Interface Anal.* **2013**, *45*, 1543.
[11] J. F. Li, Z. Q. Zheng, N. Jiang, S. C. Li, *Mater. Corros.* **2005**, *56*, 192.
[12] A. Garner, D. Tromans, *Corrosion* **1979**, *35*, 55.
[13] T. Marlaud, B. Malki, A. Deschamps, B. Baroux, *Corros. Sci.* **2011**, *53*, 1394.
[14] X. Lu, X. Han, Z. Du, G. Wang, L. Lu, J. Lei, T. Zhou, *Mater. Charact.* **2018**, *135*, 167.
[15] R. Zhang, Y. Zhang, Y. Yan, S. Thomas, C. H. J. Davies, N. Birbilis, *Corros. Sci.* **2017**, *126*, 324.
[16] R. J. Rioja, J. Liu, *Metall. Mater. Trans. A* **2012**, *43*, 3325.
[17] N. J. H. Holroyd, G. M. Scamans, R. C. Newman, A. K. Vasudevan, *Corrosion and Stress Corrosion of Aluminum-Lithium Alloys*, Elsevier Inc., London **2013**.
[18] J. A. Moreto, E. E. Broday, L. S. Rossino, J. C. S. Fernandes, W. W. Bose Filho, *J. Mater. Eng. Perform.* **2018**, *27*, 1917.
[19] P. V. Petroyiannis, A. T. Kermanidis, R. Akid, C. A. Rodopoulos, S. G. Pantelakis, *Int. J. Fatigue* **2005**, *27*, 817.
[20] M. X. Milagre, U. Donatus, C. S. C. Machado, J. V. S. Araujo, R. O. Ferreira, R. M. P. Silva, R. A. Antunes, lsolda Costa, *J. Mater. Res. Technol.* **2019**, *8*, 5916.
[21] M. Robinson, N. Jackson, *Corros. Sci.* **1999**, *41*, 1013.
[22] Y. Shi, Q. Pan, M. Li, X. Huang, B. Li, *J. Alloys Compd.* **2014**, *612*, 42.
[23] T. Marlaud, B. Malki, C. Henon, A. Deschamps, B. Baroux, *Corros. Sci.* **2011**, *53*, 3139.
[24] M. J. Robinson, *Corros. Sci.* **1983**, *23*, 887.
[25] W. Yang, S. Ji, Q. Zhang, M. Wang, *Mater. Des.* **2015**, *85*, 752.
[26] D. Tsivoulas, *Metall. Mater. Trans. A* **2015**, *46*, 2342.

[27] C. de Souza Carvalho Machado, U. Donatus, M. X. Milagre, N. V. V. Mogili, R. A. R. Giorjão, R. E. Klumpp, J. Victor de, S. Araujo, R. O. Ferreira, I. Costa, *Corrosion* **2019**, *75*, 628.
[28] T. Ramgopal, P. I. Gouma, G. S. Frankel, *Corrosion* **2002**, *58*, 687.
[29] S. Sun, Q. Zheng, D. Li, S. Hu, J. Wen, *Corros. Sci.* **2011**, *53*, 2527.
[30] R. Zhang, M. A. Steiner, S. R. Agnew, S. K. Kairy, *Sci. Rep.* **2017**, *7*, 2961.
[31] N. Nayan, M. Yadava, N. P. Gurao, S. V. S. N. Murty, S. Mahesh, M. J. N. V. Prasad, I. Samajdar, *Metall. Mater. Trans. A* **2020**, *51*, 1173.
[32] Y. C. Lin, Y.-Q. Jiang, X.-C. Zhang, J. Deng, X.-M. Chen, *Mater. Des.* **2014**, *61*, 228.
[33] Y. Deng, Z. Yin, K. Zhao, J. Duan, J. Hu, Z. He, *Corros. Sci.* **2012**, *65*, 288.
[34] M. B. Kannan, V. S. Raja, A. K. Metall, *Mater. Trans. A* **2005**, *36*, 3257.
[35] H. Li, Y. Tang, Z. Zeng, F. Zheng, *Trans. Nonferrous Met. Soc. China* **2008**, *18*, 778.
[36] S. Chen, K. Chen, G. Peng, L. Jia, P. Dong, *Mater. Des.* **2012**, *35*, 93.
[37] D. K. Xu, N. Birbilis, P. A. Rometsch, *Corros. Sci.* **2012**, *54*, 17.
[38] F. Song, X. Zhang, S. Liu, Q. Tan, D. Li, *Corros. Sci.* **2014**, *78*, 276.
[39] N. Ott, S. K. Kairy, Y. Yan, N. Birbilis, *Metall. Mater. Trans. A* **2017**, *48*, 51.
[40] D. Tsivoulas, P. B. Prangnell, *Metall. Mater. Trans. A* **2014**, *45*, 1338.
[41] Z. Ye, W. Cai, J. Li, X. Chen, R. Zhang, N. Birbilis, *Metall. Mater. Trans. A* **2018**, *49*, 2471.
[42] M. Keddam, C. Kuntz, H. Takenouti, D. Schuster, D. Zuili, *Electrochim. Acta* **1997**, *42*, 87.
[43] Y. Xu, X. Wang, Z. Yan, *Chin. J. Aeronaut.* **2011**, *24*, 681.
[44] Y. Yan, L. Peguet, O. Gharbi, A. Deschamps, C. R. Hutchinson, S. K. Kairy, N. Birbilis, *Materialia* **2018**, *1*, 25.
[45] J. Huang, J. Li, D. Liu, R. Zhang, Y. Chen, X. Zhang, P. Ma, R. K. Gupta, N. Birbilis, *Corros. Sci.* **2018**, *139*, 215.
[46] Z. Peng, Q. Pan, S. Cai, J. Li, W. Liang, *Mater. Corros.* **2019**, *70*, 2266.
[47] N. D. Alexopoulos, E. Migklis, A. Stylianos, D. P. Myriounis, *Int. J. Fatigue* **2013**, *56*, 95.
[48] T. Dorin, A. Vahid, J. Lamb, *Fundamentals of Aluminium Metallurgy*, Elsevier Inc., London **2018**.
[49] K. K. Sankaran, R. S. Mishra, *Metallurgy and Design of Alloys with Hierarchical Microstructures*, Elsevier Inc., London **2017**.
[50] J. Victor de Sousa Araujo, A. de Fátima Santos Bugarin, U. Donatus, C. de Souza Carvalho Machado, F. Martins Queiroz, M. Terada, A. Astarita, I. Costa, *Corros. Eng. Sci. Technol* **2019**, *54*, 575.
[51] ASTM G34, in *Standard Test Method for Exfoliation Corrosion Susceptibility in 2XXX and 7XXX Series Aluminum Alloys (EXCO Test)*, ASTM International, West Conshohocken, PA **2018**.
[52] ASTM G110, in *Standard Practice for Evaluating Intergranular Corrosion Resistance of Heat Treatable Aluminum Alloys by Immersion in Sodium Chloride + Hydrogen Peroxide Solution*, ASTM International, West Conshohocken, PA **2015**.
[53] Y. Ma, X. Zhou, W. Huang, G. E. Thompson, X. Zhang, C. Luo, Z. Sun, *Mater. Chem. Phys.* **2015**, *161*, 201.
[54] U. Donatus, B. V. G. de Viveiros, M. C. de Alencar, R. O. Ferreira, M. X. Milagre, *Mater. Charact.* **2018**, *144*, 99.
[55] M. X. Milagre, U. Donatus, C. S. C. Machado, J. V. S. Araujo, R. M. P. da Silva, B. V. G. de Viveiros, A. Astarita, I. Costa, *Corros. Eng. Sci. Technol.* **2019**, *54*, 402.
[56] M. Posada, L. E. Murr, C. S. Niou, D. Roberson, D. Little, R. Arrowood, D. George, *Mater. Charact.* **1997**, *38*, 259.
[57] U. Donatus, M. Terada, C. R. Ospina, F. M. Queiroz, A. Fatima Santos Bugarin, I. Costa, *Corros. Sci.* **2018**, *131*, 300.
[58] Y. L. Ma, X. R. Zhou, X. M. Meng, W. J. Huang, Y. Liao, X. L. Chen, Y. N. Yi, X. X. Zhang, G. E. Thompson, *Trans. Nonferrous Met. Soc. China* **2016**, *26*, 1472.
[59] W. Huang, Y. Ma, X. Zhou, X. Meng, Y. Liao, L. Chai, Y. Yi, X. Zhang, *Surf. Interface Anal.* **2016**, *48*, 838.
[60] X. Zhang, X. Zhou, T. Hashimoto, B. Liu, C. Luo, Z. Sun, Z. Tang, F. Lu, Y. Ma, *Corros. Sci.* **2018**, *131*, 1.
[61] W. Zhang, G. Frankel, *Electrochim. Acta* **2003**, *48*, 1193.
[62] W. Zhang, G. Frankel, *J. Electrochem. Soc.* **2002**, *149*, 1.
[63] J. F. Li, C. X. Li, Z. W. Peng, W. J. Chen, Z. Q. Zheng, *J. Alloys Compd.* **2008**, *460*, 688.
[64] R. G. Buchheit, *J. Electrochem. Soc.* **1995**, *142*, 3994.
[65] U. Donatus, R. M. P. da Silva, J. V. de, S. Araujo, M. X. Milagre, C. P. de Abreu, C. de, S. C. Machado, I. Costa, *J. Mater. Res. Technol.* **2019**, *8*, 6209.
[66] U. Donatus, L. O. Berbel, I. Costa, *Mater. Corros.* **2018**, *69*, 1375.

How to cite this article: de Sousa Araujo JV, Milagre MX, Ferreira RO, et al. Exfoliation and intergranular corrosion resistance of the 2198 Al–Cu–Li alloy with different thermomechanical treatments. *Materials and Corrosion*. 2020;71:1957–1970.
https://doi.org/10.1002/maco.202011839